PERGAMON

Journal of Structural Geology 23 (2001) 1901–1915

JOURNAL OF STRUCTURAL GEOLOGY

www.elsevier.com/locate/jstrugeo

Constraining slip rates and spacings for active normal faults

Patience A. Cowie[a,*], Gerald P. Roberts[b]

[a]Department of Geology and Geophysics, The University of Edinburgh, West Mains Road, Edinburgh EH9 3JW, UK
[b]Research School of Geological and Geophysical Sciences, Birkbeck College and University College London, Gower Street, London WC1E 6BT, UK

Received 19 June 2000; revised 6 February 2001; accepted 7 March 2001

Abstract

Numerous observations of extensional provinces indicate that neighbouring faults commonly slip at different rates and, moreover, may be active over different time intervals. These published observations include variations in slip rate measured along-strike of a fault array or fault zone, as well as significant across-strike differences in the timing and rates of movement on faults that have a similar orientation with respect to the regional stress field. Here we review published examples from the western USA, the North Sea, and central Greece, and present new data from the Italian Apennines that support the idea that such variations are systematic and thus to some extent predictable. The basis for the prediction is that: (1) the way in which a fault grows is fundamentally controlled by the ratio of maximum displacement to length, and (2) the regional strain rate must remain approximately constant through time. We show how data on fault lengths and displacements can be used to model the observed patterns of long-term slip rate where measured values are sparse. Specifically, we estimate the magnitude of spatial variation in slip rate along-strike and relate it to the across-strike spacing between active faults.

Keywords: Slip rates; Faults; Displacement

1. Introduction

The rate at which a fault slips fundamentally determines the seismic hazard that it represents because average earthquake recurrence intervals tend to decrease as slip rates increase. For this reason alone a great deal of time, money and effort is spent trying to measure slip rates and discriminate between faults that are seismically active and those that are inactive. There are relatively few areas of the earth where slip rate data are sufficient for a consensus view to emerge that can be used for seismic hazard assessment. This problem is particularly acute in low strain rate intra-plate extensional provinces. Data on slip rates for such seismically active areas are either sparse, and/or poorly constrained, and/or ambiguous.

Ambiguity may arise because independent workers or research groups may collect slip rate data using different methods. For example, for a single area like the Italian Apennines, rates have been estimated by trenching and dating fault scarps (e.g. Michetti et al., 1996; Pantosti et al., 1996; Galadini et al., 1997), or using geomorphic evidence such as triangular facets and scarps along range fronts (e.g. Piccardi et al., 1999). These estimates can provide average rates of slip over time periods of 10^4–10^5 years. In the case of a trench, the derived rate is constrained at just that one point along the scarp. This can lead to different slip rates being proposed for the same fault if trench sites are chosen at different positions relative to the point of maximum displacement on that fault (e.g. compare Michetti et al. (1996), Pantosti et al. (1996) and Galadini et al. (1997) for a single fault in central Italy; see Section 4.1.1). Slip rates derived from geomorphic observations may also vary compared with those from trenches for the reason just stated, or may overestimate or underestimate slip rates compared with those from trench sites even when observed close to trench sites (e.g. Piccardi et al. (1999) for geomorphic observations of the same fault as that studied by Michetti et al. (1996) and Pantosti et al. (1996) in central Italy). This is because there is no guarantee that slip rates for the last few thousand years derived from trenches will match those for geomorphic observations of features that have taken tens of thousands of years to form if the fault has experienced temporal earthquake clustering (in the sense of Sieh et al. (1989) and McCloskey and Bean (1994)). In any case, landscape evolution models have called into question the basis for deriving slip rates directly from geomorphic features such as triangular facets (Ellis et al., 1999; DePolo and Anderson, 2000).

Alternatively, geodetic measurements and earthquake

* Corresponding author. Fax: +131-668-3184.
E-mail address: cowie@glg.ed.ac.uk (P.A. Cowie).

0191-8141/01/$ - see front matter
PII: S0191-8141(01)00036-0

moment summations are now routinely used to calculate regional strain rates (e.g. Clarke et al. (1997), Davies et al. (1997) and Kahle et al. (2000), for the Gulf of Corinth, Greece). These methods rely on data covering only the last few decades or centuries. For the Gulf of Corinth, relative geodetic site velocities generally overestimate slip rates measured on specific faults (see Doutsos and Poulimenos, 1992; Collier et al., 1998). Again, this may be because workers are measuring different things due to: (1) the large differences in baseline lengths between geodetic surveys (tens of kilometres) and trench sites (tens of metres), or (2) base-lines crossing individual faults in different positions relative to the point of maximum displacement on the fault. As with comparing trenching and geomorphic results, one is left to choose between conflicting slip rate data.

Slip rates have also been estimated from sediment thicknesses and stratal tilts in fault-controlled basins (e.g. Anders et al., 1989; Nicol et al., 1997; Contreras et al., 2000; McLeod et al., 2000). This latter approach provides estimates of average rates of slip over very long timescales, i.e. $>10^5$–10^7 years. These long time period measurements may be, at present, the best way to derive slip rates that are representative of the long-term seismic hazard. However, it is rare for such measurements to be available, or of sufficient quality, in actively-deforming regions that have not been subjected to recent hydrocarbon exploration studies. For example, for the seismically active areas of central Greece and central Italy such data are unavailable. Where such data do exist they can show conflicting results with long-term slip rates in some cases changing while in other cases remaining constant through time (e.g. compare Nicol et al. (1997) with Contreras et al. (2000), McCalpin (1993) and Wallace (1987)). Consequently, it is unclear whether one is able to simply assume that long-term rates are the same as present-day rates in being responsible for seismic hazards. Also, the age resolution of the strata and dating constraints determine whether any temporal variations in slip rate can be detected such as that expected if earthquakes show temporal clustering (e.g. Dorsey et al., 1997). This is another reason why it is difficult to compare such rates with those measured over short-timescales (e.g. from geodesy, earthquake moment summation, geomorphology or trench site observations). A further complicating factor, and one that cannot easily be quantified, is that all the above types of study may be subject to interpretation errors which may lead to incorrect slip rates.

For all of the above reasons it is quite common to have a number of differing slip rate estimates available for a fault that poses a potential seismic hazard. One is left with a subjective, and therefore difficult, decision concerning which is the appropriate rate to use in assessing seismic hazard. What is needed is an objective method that helps one decide which rate is most likely to represent the long-term seismic hazard.

The aim of this paper is to demonstrate that, in addition to direct field measurements, independent constraints on fault slip rates can be derived from considering how faults grow over their entire lifetimes. The idea we present relies heavily on the observed relationship between the maximum displacement on a fault and its length, and the growth processes that underlie this relationship. Most of the recent understanding of the scaling relationship between displacement and length is based on observations of extensional faults (see Cowie (1998a) for review). Consequently, the work presented here concerns normal faults exclusively. We show that the way in which normal faults grow inevitably leads to significant slip rate variations: (1) along strike, (2) across strike, and (3) with time. Furthermore, we show that simple fault-scaling arguments allow the variations to be quantified. Our model is based on current understanding of the mechanics of fault interaction and linkage. Thus, it provides a physical framework in which existing empirical slip rate data can be assessed and compared, sparse data sets can be extrapolated, and future data collection can be planned.

2. Displacement–length scaling during growth by linkage

In extensional settings, linkage of faults has been shown to be an important fault growth mechanism (e.g. Cartwright et al., 1995). Growth by linkage produces rapid increase in fault length, L. Dawers and Anders (1995) showed that in time this length increase is matched by accumulation of displacement, d, so that overall the scaling relationship $d = \gamma L$ for the linked fault array is re-established. When averaged over eight orders of magnitude of fault data d~$0.03L$ (Schlische et al., 1996), but typically γ shows a wide range from 0.001 to 0.1. The range partly reflects variations in local rock type, friction on the fault surface, and the three-dimensional (3D) shape of the faults (e.g. Cowie and Scholz, 1992; Burgmann et al., 1994; Willemse et al., 1996; Willemse, 1997). However, several authors have demonstrated that pre-linkage fault interaction combined with post-linkage displacement readjustment strongly influences the measured displacement–length ratio (Peacock and Sanderson, 1991; Cartwright et al., 1995; Willemse et al., 1996; Willemse, 1997; Gupta and Scholz, 2000). It is these interaction-readjustment phenomena, and the development of a range of γ values in a single extensional province that we quantify below, allowing us to objectively assess various slip rate measurements.

Displacement measurements along the Strathspey–Brent–Statfjord fault in the northern North Sea (Fig. 1) provide a particularly well-documented example of growth by linkage in association with profile readjustment along a crustal-scale fault. The evolution of this structure through time has been mapped out by McLeod et al. (2000) using 3D seismic data, well logs and core. The throw profile shown in Fig. 1 extends from the centre of the fault (which is ~100 km long) to its northern tip. McLeod et al. (2000) show that the present-day length of the fault was established early on by

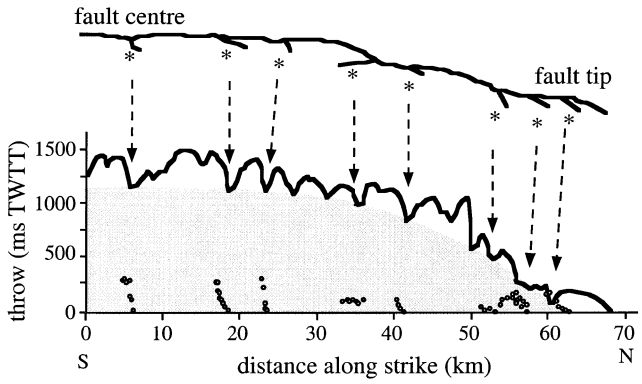

Fig. 1. Fault trace map (top) and throw profile in two-way travel time along the Strathspey–Brent–Stafjord fault in the north North Sea, modified from McLeod et al. (2000). Stars indicate the locations of segment boundaries and intrabasin highs along the fault. Grey shaded area indicates the throw accumulated post-linkage. The circles indicate throw on the splay faults, which represent the paleosegment tips (see McLeod et al. (2000) for full details). Arrows relate segment boundaries to displacement minima.

linkage of segments along-strike. The irregularities seen in the throw profile (see Fig. 1) are not due to erosion of the foot wall as this fault formed in a submarine environment. Instead, McLeod et al. (2000) have shown that each local throw maximum coincides with the centre of a relict fault segment. The throw minima correspond to relict segment tips and the location of intra-basin highs separating sub-basins in the hanging wall.

An analysis of the throw-length ratios shows that the relict segments are self-similar with the present-day structure (McLeod et al., 2000). However, immediately post-linkage the throw profile was extremely 'under-displaced' (as defined by Cartwright et al. (1995)), having a total length of ~100 km but with only a few hundred meters of maximum displacement. By mapping out the thickness variations and on-lap relationships in the syn-rift strata, McLeod et al. (2000) have been able to constrain the timing of segment linkage and quantify the rate of fault displacement and how it varies through time. They demonstrate that at the time of segment linkage the throw rate near the centre of the fault increased from about 0.055 mm/year to >0.092 mm/year. The increase in throw rate is evident from Fig. 1 because the unshaded and shaded areas of the throw profile represent approximately equal intervals of time, i.e. ~10 my (McLeod et al., 2000). By comparing the shaded and unshaded areas of Fig. 1, it is also evident that the increase in throw rate at the time of linkage diminishes towards the end of the linked structure. In fact the most distal segment shows little evidence of post-linkage displacement accumulation (Dawers and Underhill, 2000). It is this increase in the throw-rate at the centre of the linked structure that allowed it to develop a throw/length ratio self-similar with the early, individual fault segments. Furthermore, McLeod et al. (2000) demonstrate that the timing of segment linkage and throw rate increase coincided with cessation of activity on faults in the hanging wall to the Strathspey–Brent–Statfjord fault. This cessation of activity on hanging wall faults is thought to have allowed a constant regional strain rate to be maintained as the slip rate increased on the Strathspey–Brent–Statfjord fault. The above observations show that slip rates vary both spatially and temporally during the lifetime of a fault as it grows by linkage. It is these variations that we attempt to model below.

The Strathspey–Brent–Statfjord example illustrates that a fault growing by linkage re-adjusts its displacement profile through time and re-establishes the displacement–length ratio that existed prior to linkage. Note that growth post-linkage occurs primarily by displacement accumulation with no lengthening (see Morewood and Roberts (1999), Morley (1999) and Poulimenos (2000) for other field examples of this). The tips of the newly formed linked structure cease to propagate because the displacement gradient from the centre of the linked fault to the tip has been dramatically reduced. Until the gradient has been re-established the tip stress concentration is insufficient to drive further propagation (see Cowie and Shipton, 1998). Another important feature to note is the increase in the rate of slip that is associated with linkage. In order to maintain constant regional strain rate there must be cessation of activity on adjacent faults in the foot wall and hanging wall areas of the linked structure as its slip rate increases (Gupta et al., 1998). Finally, the variation in post-linkage slip rate along strike determines the displacement profile shape that is ultimately achieved. The implication of this last point is that the number of faults in foot wall and hanging wall areas that become inactive will also vary along strike, mirroring the variation in post-linkage slip rate.

3. Physical mechanisms

A physical mechanism has been proposed to explain how displacement profile re-adjustment occurs during growth by linkage (Cowie, 1998b). This work presents numerical simulation of elastic-brittle deformation that produces an evolving fault population (see Cowie et al. (1993) for discussion of the model). The mechanism, which is simulated in the model, is based on the observation that changes in stress during normal faulting earthquakes increase the stress levels along-strike. This can advance the timing of future earthquakes on neighbouring along-strike faults (Hodgkinson et al., 1996; Caskey and Wesnousky, 1997). A positive feedback situation occurs, because a ruptured fault, once healed, can be partially reloaded towards failure by subsequent earthquakes, especially by those earthquakes triggered on along-strike faults. Thus, the central segments of a linking fault array are reloaded more often, and consequently experience more frequent earthquakes and higher slip rates compared with the distal segments (Cowie, 1998b). This mechanism can explain the pattern shown in Fig. 1. It may also explain the palaeoseismological data of

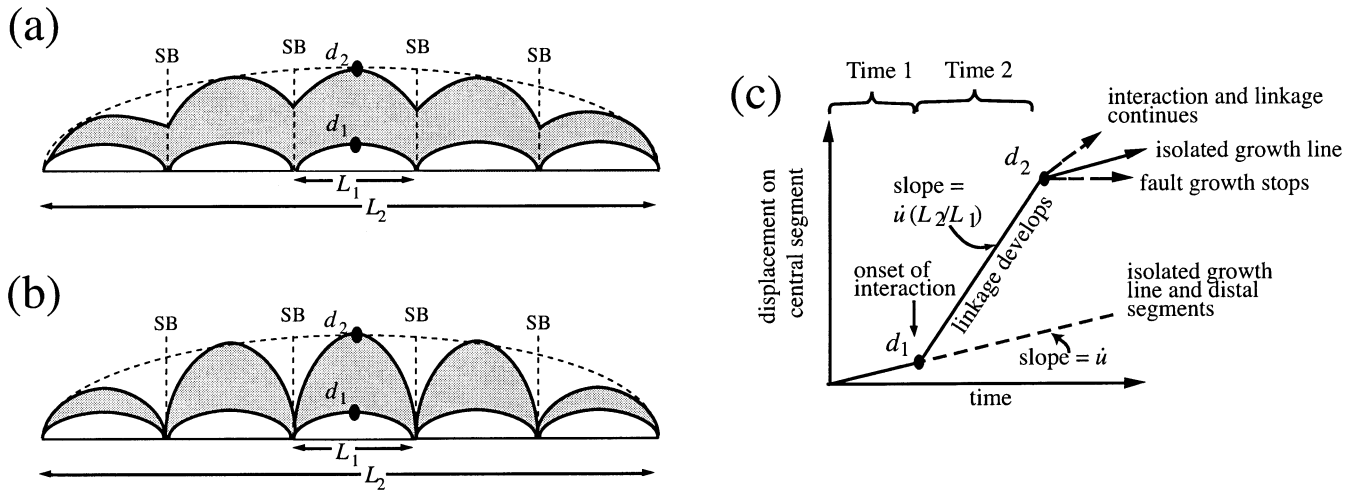

Fig. 2. Growth of an idealized extensional fault array. (a) Displacement profiles prior to interaction, and after displacement profile re-adjustment is complete, showing how fault scaling arguments imply that central faults must have an enhanced slip rate relative to distal faults (SB = segment boundary). In (a) fault linkage occurs at the onset of profile re-adjustment. (b) Same as (a) except that linkage occurs late in the profile re-adjustment history. (c) Displacement as a function of time on the central faults shown in (a) and (b) showing the enhanced rate of growth as interaction and linkage proceed (see text for explanation). Time 1 refers to the period prior to significant interaction. Time 2 refers to the time period over which the slip rates vary along the fault array. Actual linkage of the faults may occur at any time during this latter period; scenarios (a) and (b) show the two end-members.

Machette et al. (1991) along the Wasatch fault in Utah, which show that the central segments are slipping at rates of >1 mm/year whereas the rates on the distal segments are <0.5 mm/year. A similar pattern has been noted by Byrd et al. (1994) for the Teton fault in Wyoming.

Cowie (1998b) also discusses the effect of negative stress feedback on an evolving population of faults. This situation arises because, in addition to along-strike stress enhancement, a normal faulting earthquake creates stress shadows in foot wall and hanging wall areas (Hodgkinson et al., 1996). Consequently faults that have mutually overlapping stress shadow zones experience negative stress feedback. Cowie (1998b) shows that, depending on the location and orientation of a fault with respect to its neighbours, a fault may either grow very rapidly if it experiences strong positive stress feedback, or exhibit a slow growth rate and eventually become inactive if it falls within a shadow zone. This explanation agrees well with the observations of Nicol et al. (1997) who used seismic and well data to demonstrate marked differences in rates of growth of normal faults that formed at the same time during the same extensional episode. More field evidence for cessation of activity of faults in the foot wall and hanging wall areas of larger active structures is summarised by Jackson (1999) for mainland Greece and by Sharp et al. (2000) for the Suez rift (see also McLeod et al., 2000).

Such slip rate variations along normal faults are well explained in terms of the stress feedback mechanism described above, but do not depend on this as the exclusive physical explanation. Willemse et al. (1996) and Willemse (1997) propose static elastic interactions to explain variations in displacement–lengths ratios along fault arrays. They use a boundary element model in which the dimensions of the fault segments comprising the arrays are predefined and fixed. Their results are qualitatively comparable with those of Cowie (1998b) but do not explicitly show fault array growth as a function of time and slip rates cannot be directly derived. However, a disadvantage of the results described by Cowie (1998b) is that the numerical simulations may be only qualitatively compared with real fault data rather than quantitatively applied to specific areas of active deformation.

4. Slip rate variations along-strike

Our aim here is to show how relatively simple field measurements may be used to quantify along-strike variations in fault slip rate necessary for profile readjustment. We argue that the empirically established scaling relationship, $d = \gamma L$, can be used to infer the magnitude of the variation regardless of the underlying mechanism. Fig. 2 illustrates an idealised fault array consisting of N segments of equal length L_1 that link up to form a single larger structure of length L_2. Prior to linkage the displacement on each fault is given by $d_1 = \gamma L_1$ whereas the displacement–length ratio for the incipient linked array is $\gamma L_1/L_2$, i.e. it is underdisplaced. As interaction and linkage proceed, the profile of the entire fault zone re-adjusts until the maximum displacement approaches a value given by $d_2 = \gamma L_2$, self-similar with the original unlinked faults (Fig. 2).

In order to produce the new profile shape along the linked array, the slip rate must vary along strike. For the example given in Fig. 2 it is clear that higher rates will develop along

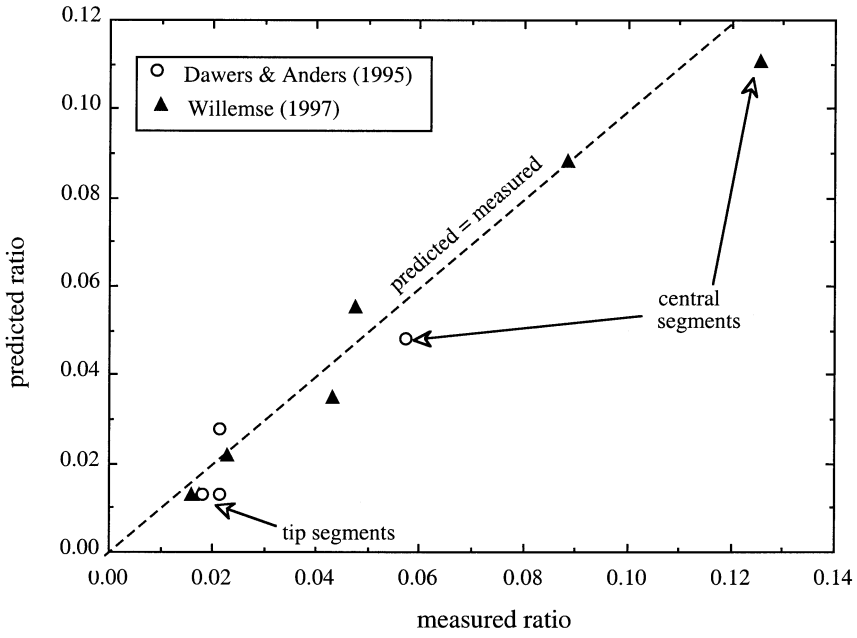

Fig. 3. Comparison between predicted and measured displacement–length ratios along two fault arrays in the Volcanic Tableland, eastern California. The data come from Dawers and Anders (1995) and Willemse (1997). Dashed line is shown as a reference line indicating a one-to-one correlation; it is not a regression through the data points.

the central portion of the array relative to the distal portions. For example, if the slip rate on the most distal segments is $\dot{u}$, the slip rate on the central segment must be $\dot{u}(L_2/L_1)$ in order that a displacement d_2 is achieved at the centre of the array (Fig. 2c). We call the ratio L_2/L_1 the slip rate enhancement factor, E, for the central segment. How much the slip rate increases towards the centre is controlled by how much the profile needs to re-adjust to achieve the new shape and thus it depends on the original lengths and displacements as well as the positions of segments comprising the array. In Fig. 2 the array is symmetrical about its mid-point and all the segments have the same length, but this need not be the case as we show below. Our method assumes only that a fault growing by linkage will develop such that it re-establishes a displacement–length ratio, γ, and profile shape that are consistent with the rock type and tectonic setting in which it is growing (Dawers and Anders, 1995). The slip rate variations in time will persist until this displacement re-adjustment is achieved (Time 2 in Fig. 2c).

The timing of profile re-adjustment relative to actual structural linkage between segments does not affect our calculations. Pre-linkage interaction may account for much of the re-adjustment, as shown by Willemse (1997); and Gupta and Scholz (2000), in which case considerable distributed deformation and tilting may occur in the relay ramps between the segment tips (e.g. Dawers and Anders, 1995). Alternatively, Cartwright et al. (1995) found evidence in the Canyonlands field area, Utah, for linkage preceding significant displacement re-adjustment. Consequently, in Fig. 2 we show two end-member scenarios: (1) an end-member where linkage coincides with the onset of enhanced slip rates (Fig. 2a), as shown by McLeod et al. (2000) (see Fig. 1); and (2) an end-member in which linkage occurs late in the history of profile re-adjustment (Fig. 2b).

After linkage, the length, L_1 of the original faults can still be determined from the spacing of segment boundaries (SB; Fig. 2), which often correspond with intra-basin highs separating sub-basins in the hanging wall (Anders and Schlische, 1994; McLeod et al., 2000). The L_1 lengths will also be defined by the directions of striations on exposed fault surfaces (Roberts, 1996): at the tips of extensional faults, the striations are deflected systematically from the expected down-dip direction. Sites of fault linkage are also commonly associated with local displacement minima as shown in Fig. 1 (Cartwright et al., 1995; McLeod et al., 2000). We use some or all of these criteria in the examples below to define the lengths of fault segments prior to and subsequent to linkage. Note that segment boundaries, as we define them, do not necessarily correlate with barriers to seismic rupture (Anders and Schlische, 1994), although for some earthquakes the two may coincide (DePolo et al., 1991). The length L_1 may be mechanically controlled by the thickness of the seismogenic layer as suggested by Jackson and White (1989). An upper limit to the length L_2 is determined by the maximum fault topography (i.e. d_2) that can be supported by the flexural strength of the lithosphere (Hayward and Ebinger 1996; Scholz and Contreras, 1998).

We calculate the enhancement factors E for individual segments within an array, and thus the spatial variation in slip rate along strike, by considering the shape of the displacement profile and the length of each segment compared

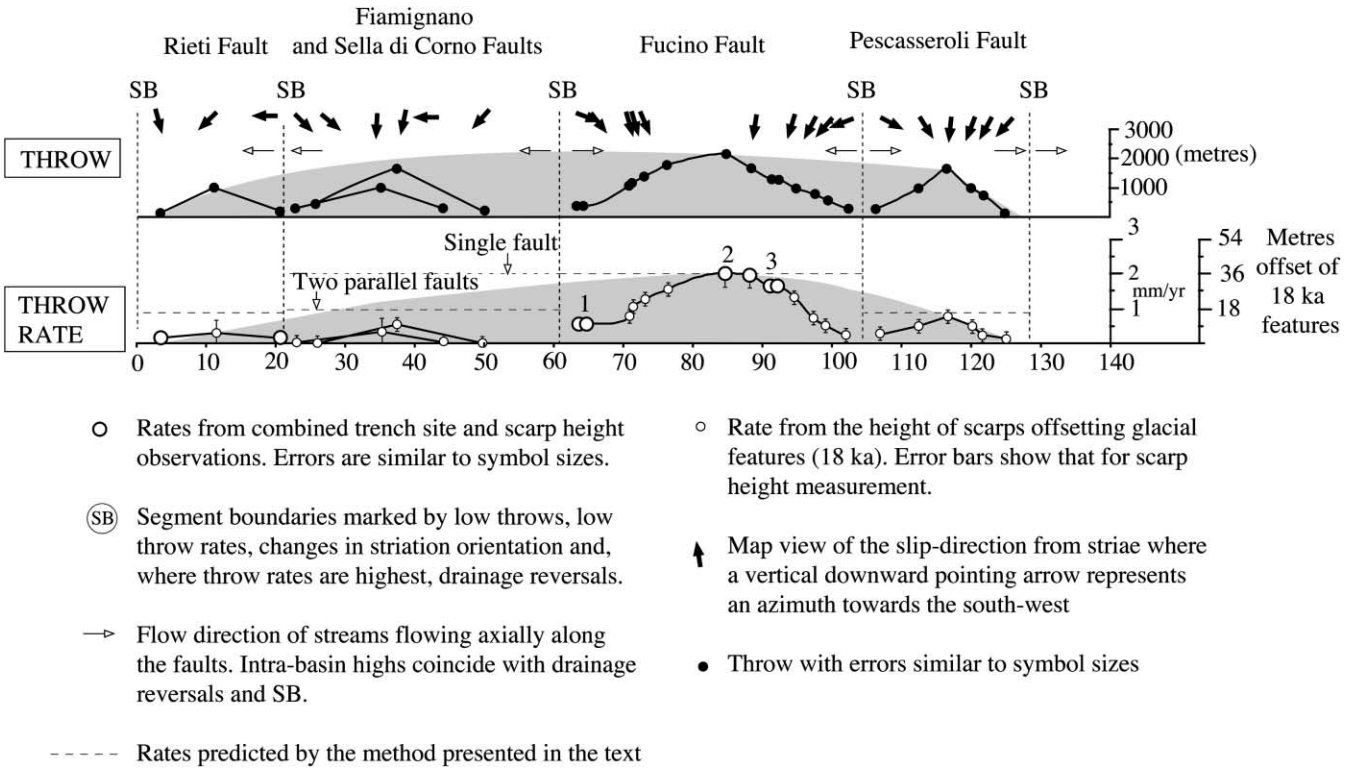

Fig. 4. Throw and slip rate versus distance along an extensional fault array in central Italy. Slip rates from trenching of Holocene sediments (Michetti et al., 1996; Pantosti et al., 1996; Galadini et al., 1997), and offset features associated with the c. 20–16 ka glacial retreat phase (Giraudi and Frezzotti, 1997). Error bars shown for scarp height measurements (<0.2 mm/year). Fault tips are defined by throw minima, changes in throw rate magnitude, and slip-directions which deviate from down-dip. Predicted throw rates are shown for comparison. Numbered slip rates shown in lower panel are from: (1) Pantosti et al. (1996); (2) Michetti et al. (1996); (3) Galadini et al. (1997). The rates shown at these three points are that of the above mentioned authors plus that of nearby fault scarps.

with the length of the final linked array. Fig. 2a and b shows an elliptical profile shape with segment length L_1 a constant along the array. In this case the slip rate required to re-adjust the profile will vary according to the equation for an ellipse, i.e. $(1 - 4(L_2/2 - R_i)^2/L_2^2)^{1/2}$ where R_i is the distance between the mid-point of each segment and the nearest tip of the overall array. Note that we calculate E only at the segment mid-points and we assume that the values are representative of the slip rate along each segment. A simpler expression is obtained if instead we assume that the displacement profile is triangular in shape, i.e. decreasing linearly from a maximum value at the centre to zero at the tips. In this case, E is given by $2R_i/L_i$ where L_i is the length of the ith fault segment. In Fig. 3 we test the validity of making this linear approximation for two data sets. Both data sets have been collected from the Volcanic Tableland area in eastern California and they consist of measurements of cumulative displacement along fault arrays. The lengths, L_i, of the segments comprising these arrays are defined by displacement minima. For each data set we have calculated a displacement–length ratio for each segment and plotted it against the measured ratio (Fig. 3). The calculated ratio is obtained by computing the normalised enhancement factor $2R_i/L_i$ for each segment in turn and multiplying this value by the displacement–length ratio ($=0.013$) measured for relatively isolated, single faults in this area (Dawers et al., 1993). Note that because $R_i = L_i/2$ for the most distal segments, our calculation predicts $E = 1$ (and thus a displacement–length ratio $= 0.013$) for the segments at the array tips.

Fig. 3 shows that for these data sets the linear approximation is valid and consequently we apply it in the examples presented below. Note that it is not necessary to make this approximation if there is clear evidence for a non-linear profile shape. For the examples we studied we found that the largest discrepancies caused by using a linear rather than an elliptical profile shape were at the tips of the array rather than at the centre. Because the slip rates at the array tips are very low (e.g. Fig. 1) this discrepancy is less important in terms of seismic hazard. It is the higher rates, which occur along the central segments that are much more important to constrain.

In this calculation we also neglect to consider variations in down-dip dimensions of the fault plane that may occur during linkage, although we discuss the impact of this process on strain partitioning (Section 5). Willemse (1997) has shown that down-dip fault width influences the displacement–length ratio (see also Dawers et al., 1993;

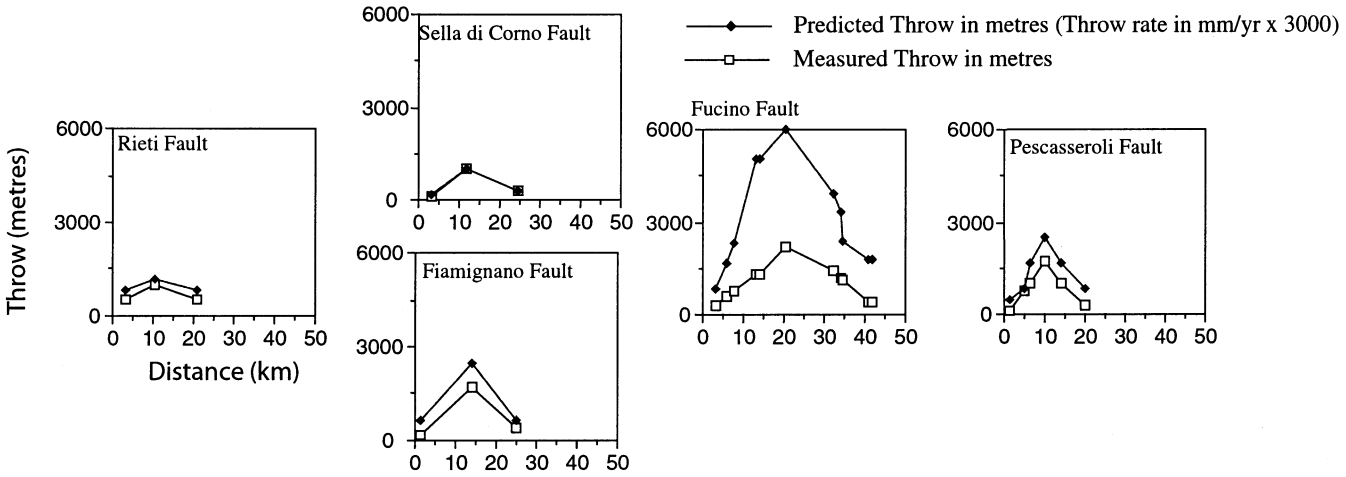

Fig. 5. Comparison between observed and predicted throw along-strike for the fault array shown in Fig. 4. Predicted throws are obtained by projecting present-day throw rates over a time period of 3 Ma, which is the age of the faults. Note that the predicted throw exceeds the observed throw for all of the fault segments and the difference is greatest for the Fucino fault.

Gudmundsson, 2000). Our point of view is that a linking fault array may well continue to propagate down dip and increase its down-dip width as the displacement profile re-adjusts. This is physically reasonable because the down-dip displacement gradient has not been modified by along-strike linkage. However, the observation that displacement and length correlate over eight orders of magnitude (Schlische et al., 1996) indicates that down-dip width is not the controlling dimension. Moreover, the field examples that we present later in this paper are all for faults with lengths much greater then the thickness of the layer in which they have developed, e.g. the thickness of the brittle crust. Down-dip width is therefore likely to have an upper limit whereas along-strike linkage, and thus length, is not limited if foot wall erosion counter balances the creation of new topography by fault growth (King and Ellis 1990). If down-dip width were the controlling dimension, the published slip rate variations shown here could not be explained by our model. In contrast, using length as the controlling dimensions produces good results (see below). If needed, modifications to the displacement profile shape caused by finite down-dip width may easily be incorporated into our approach by deriving the appropriate formula for E, for example using profile shape data from Dawers et al. (1993).

4.1. Applications

In the above sections we have reviewed the evidence and physical basis for observed variations in displacement–length ratios along the strike of extensional fault arrays as they develop. In this section we show how the slip rates implied by these variations can be used as an independent constraint on rates measured in the field (Figs. 4–7).

4.1.1. Lazio–Abruzzo, central Italy

Our first example is from Lazio–Abruzzo in central Italy, which is being actively extended in a NE–SW direction (Figs. 4 and 7a). We present new data on the fault system so our account is necessarily longer than that for the following two examples. Our studies have constrained the kinematics for most of the active faults in the region and we have finite throw and throw-rate data for some of the active normal faults. We collected data concerning: (1) throw, through construction of serial cross-sections, (2) slip-directions, through measurement of striated faults at outcrop, and (3) throw rates, through study of the heights of scarps offsetting deposits and landforms produced by the main glacial retreat phase (c. 16–20 ky), and from published palaeoseismological trench site data (Fig. 4) (Table 1). The data will be presented in detail elsewhere. We have found that: (1) a number of parallel active faults exist in the region; (2) along-strike linkage is incipient (i.e. the faults are soft-linked); (3) both the throws and throw-rates are greatest for faults located centrally within the fault array; and (4) throw rates appear to have increased with time, with the effect most marked on the longest, centrally located fault (Fig. 5). The clear correlation between throws and throw rates suggests that the scarps have not been produced or affected by erosion (Galadini, 1999). The throw rates from scarps also correlate with, and explain, differing rates derived from trench observations at different localities along the faults. We give details of our observations below.

It is clear from historical seismicity, our observations of offset post-glacial features and published palaeoseismological trench site data (Michetti et al., 1996; Pantosti et al., 1996; Galadini et al., 1997; Giraudi and Frezzotti 1997) that parallel faults are active in Lazio–Abruzzo. Throw and throw rate profiles decrease to zero values between both en échelon or end-to-end fault tips, so the faults have not yet linked. This is consistent with a detailed study of one of the segment boundaries (Morewood and Roberts, 2000).

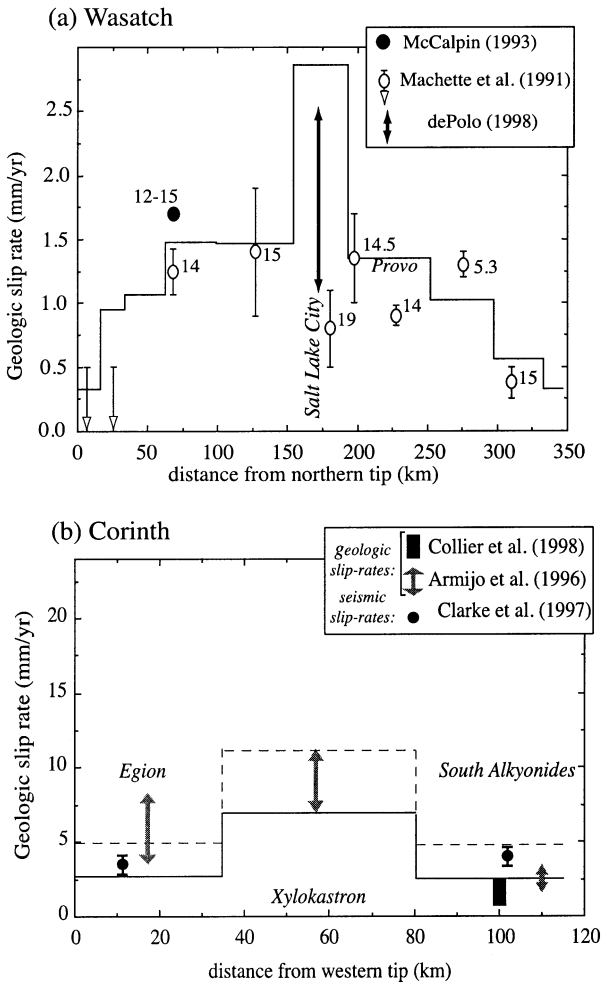

Fig. 6. Predicted slip rates compared with observations for: (a) Wasatch fault, Utah (data from Machette et al. (1991, 1992) and refs therein, McCalpin (1993) and dePolo (1998)). Numbers in bold indicate age (in ky) of offset deposit on which slip rate is based; most ages are early Holocene. (b) Gulf of Corinth, Greece. Geological data from Armijo et al. (1996) and Collier et al. (1998). Seismic moment release rates from Clarke et al. (1997). Solid and dashed lines indicate lower and upper rate predictions, respectively.

These along-strike variations in throw and throw rate produce fault-parallel (i.e. NW–SE) stretching, in turn producing a pattern of slip that converges towards the fault centres (Roberts, 1996), and minor faults in segment boundaries, such as the Velino–Magnola fault (VMF, Fig. 7a), which accommodate local N–S to NW–SE extension within the segment boundaries (Morewood and Roberts, 2000). The converging slip patterns occur over length scales identical to the throw and throw rate variation along individual faults. Thus, the kinematic data, alongside the throw and throw rate data, help us confirm the L_1 lengths of these structures. This is because the inward-pointing slip patterns are produced by throw gradients (Roberts and Ganas, 2000) and are therefore consistent with the throw and throw rate data. This gives us confidence that our throw and throw rate profiles are correct (Fig. 4). Note that our throw and throw rate measurements underestimate the displacements near the fault tips by a few tens of percent due to oblique slip at these localities (slip-directions pitch less than ~45° in the plane of the main fault). However, because throw and throw rate change along the length of individual faults by up to a factor of $\times 10$, this makes no difference to our conclusions: the displacement and displacement rate minima are located in the same positions as the throw and throw rate minima. We choose to show throw values instead of displacement values so our data can be compared with less complete datasets which do not include kinematic measurements of oblique slip at fault tips.

The faults began to form at about 3 Ma (Cavinato and de Celles, 1999), so we have projected the present-day throw rates over a time period of 3 Ma to predict how much throw would have accumulated if throw rates had remained constant (Fig. 5). We note that the predicted throw values are larger than the measured throw values. The biggest discrepancy between these profiles exists for the longest, centrally-located Fucino fault (Fig. 5). Even if we use 2 or 4 Ma as the age of fault initiation we achieve a similar pattern of discrepancy between predicted and measured throws. We interpret this to indicate that the throw rates have increased with time with the largest increase for the Fucino fault. This resembles the pattern described by McLeod et al. (2000) (see Fig. 1), and the model shown in Fig. 2. Specifically, the patterns of throw, throw rate and throw rate increase through time resemble that which we suggest will occur in Time 2 of our growth model.

The length and geometry of the L_2 structure is more difficult to determine. The faults for which we show throw and throw-rate profiles lie along strike from each other, forming a single footwall mountain range. Our cross-section constructions and scarp observations show that no other active faults exist immediately to the SE or NW beyond the array tips. The largest throws and highest throw rates (during the last 16–20 ky) occur towards the centre of the array (Fig. 4). Thus, in our first attempt to predict deformation rates, we assume that the faults between the NW tip of the Rieti fault and the SE tip of the Pescasseroli fault form a single array ($L_2 = 130$ km; see discussion below). This assumption is based on our belief that the faults, although not yet linked, are interacting and behaving as if they were a single larger fault, as illustrated in Fig. 2b. Thus, with values for both the L_1 and L_2 lengths, spatial variation in slip rate along this array can be modelled by calculating the throw rate enhancement (vertical component of slip rate enhancement), E, for each fault (as described above).

The predicted rates, which compare well with the measured rates, were obtained by normalizing each enhancement factor to that of the Fucino fault and multiplying by its well-constrained throw rate (2 mm/year; derived from the trench investigations of Michetti et al.

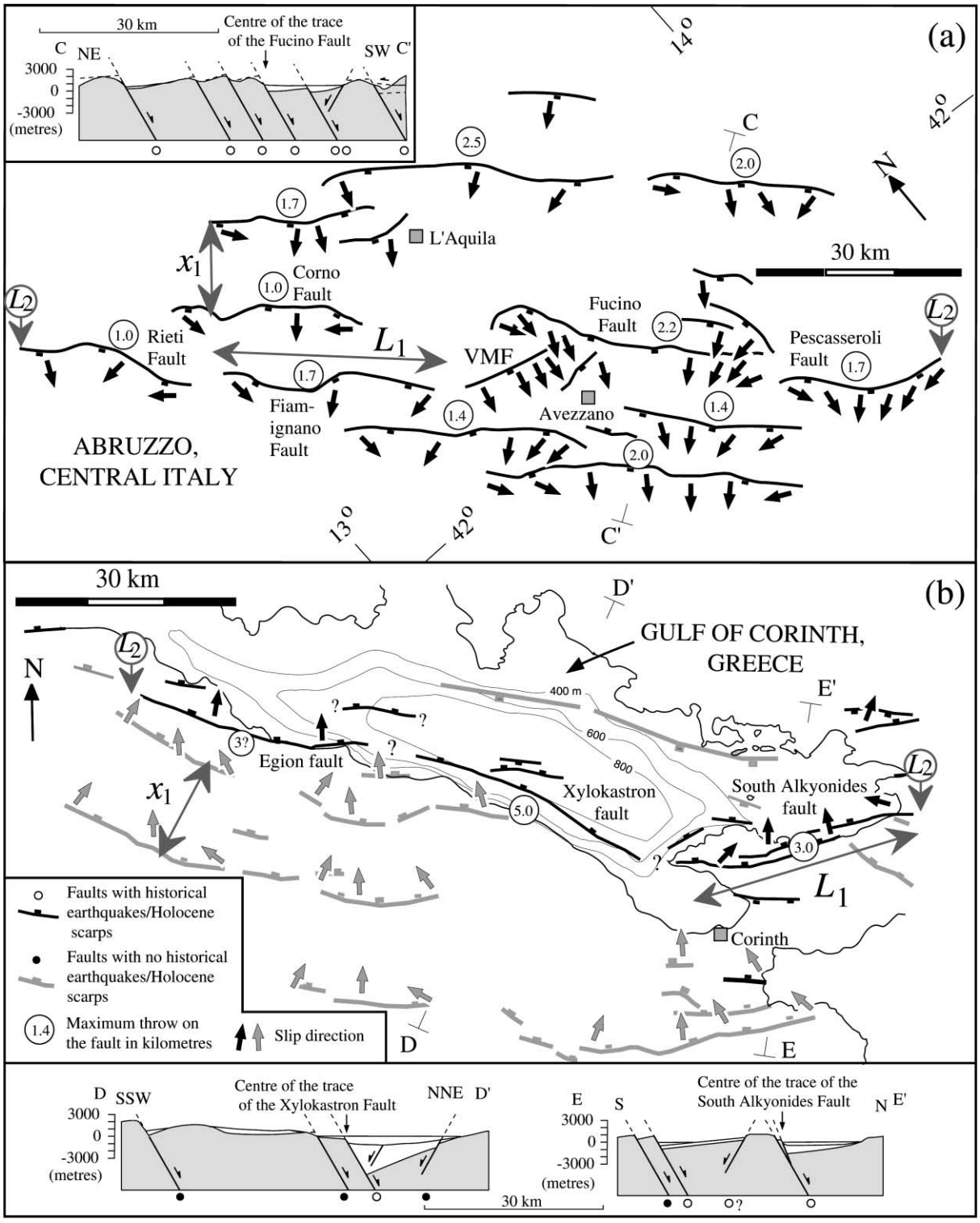

Fig. 7. Comparison of active fault spacing between two actively extending areas: central Italy and Gulf of Corinth, Greece. In (a) VMF is the Velino–Magnola fault referred to in the text. In central Italy the faults all show Holocene activity, whereas in mainland Greece recent fault activity is localised along the Gulf of Corinth and the Gulf of Evia to the north. Distance x_1 is the spacing of initial fault lengths, L_1. As the displacement profile readjusts from d_1 to d_2 the maximum spacing between active faults increases from x_1 to x_2. See text for explanation.

Table 1
Data plotted in Fig. 4. Numbers in left hand column indicate localities at which striation data were collected. Each black arrow shown in Fig. 4 represents one locality. The locality numbers 1 through 25 refer to successive arrows from left to right in Fig. 4

	Fault	Nearest town or geomorphic feature of note	X UTM coordinate	Y UTM coordinate	Slip direction mean (degrees)	Plunge of slip vector (degrees)	Throw derived from cross-sections (m)	Throw rate from scarp heights and trench data (mm/year)	Distance along fault (km)
1	Rieti	Reatino	323500	4711000	205	46	500	0.27	21.0
2		Lisciano	329000	4703000	266	82	1000	0.4	10.5
3		Cittaducale	332000	4695000	310	59	500	0.27	3.0
4	Sella di Corno	Micigliano	340759	4701283	170	55	300	0.10	24.5
5		Sella di Corno	347049	4695166	223	57	1000	0.33	12.0
6		La Forco	354950	4685754	310	45	100	0.05	3.0
7	Fiamignano	Pendenza	337173	4690531	175	39	400	0.22	25.0
8		Fiamignano	345000	4682000	232	51	1700	0.83	14.0
9		Corvaro	355500	4674500	262	67	200	0.22	1.5
10	Fucino	Piano di Pezza 2	373504	4672145	151	59	400	0.60	42.0
11		Piano di Pezza 1	373504	4672145	182	44	400	0.60	41.0
12		Ovindoli 2	377014	4665929	204	50	1100	0.80	34.5
13		Ovindoli 1	377014	4665929	204	42	1200	1.10	34.0
14		S. Potito	377544	4664498	197	65	1400	1.30	32.3
15		S. Benedetto–Parasano–Ventrino	391544	4658336	215	49	2200	2.00	20.5
16		Venere	389418	4647451	229	59	1300	1.68	14.0
17		Gioia dei Marsi	393500	4645000	248	71	800	0.77	7.8
18		Sperone	395000	4643700	261	72	600	0.55	6.0
19		Valico di Gioia Vecchio	394927	4640055	289	43	300	0.30	3.0
20	Pescasseroli	Morrone del Diavolo	397490	4635700	158	68	300	0.30	20.0
21		La Canala	401500	4631200	188	51	1000	0.55	14.0
22		Opi	403875	4627983	226	64	1700	0.83	10.0
23		M. Forcone	407351	4626281	241	9	1000	0.55	6.5
24		Villeta Barrea	408903	4626329	249	27	800	0.27	5.0
25		C. Alfadena	411513	4624397	262	32	100	0.16	1.5

(1996) and geomorphic investigations, which reveal 1.6 mm/year from the trench plus 0.4 mm/year implied by nearby scarps) (Fig. 4). In one place we show the predicted rate divided by two because two parallel faults exist, the Sella di Corno and Fiamignano faults, and the deformation appears to be distributed between them (Morewood and Roberts, 2000). Thus, despite the fact that we have ignored other across-strike faults which we know are active (see Fig.7a), our approach has provided a reasonable prediction of the slip rate variation that compares well with measured values. With more data concerning the faults located across strike, we will be able to improve our analysis; this work is underway. However, we argue that: (1) the agreement between observed and predicted throw rates, (2) the similarity in profile shape shown in Figs. 2b and 4, and (3) the change in throw rate with time in Lazio–Abruzzo (Fig. 5), are strong evidence for a fault-scaling control on the rate variations. Furthermore, this example supports the idea that some displacement profile re-adjustment occurs before complete structural linkage is achieved, as described by Peacock and Sanderson (1991), Willemse (1997), Dawers and Anders (1995) and Gupta and Scholz (2000). This is the first time, to our knowledge, that the phenomenon of pre-linkage displacement profile re-adjustment has been demonstrated for a crustal-scale fault.

4.1.2. Wasatch fault, Utah, USA

We have also studied the Wasatch fault in Utah using the segmentation pattern of Machette et al. (1991) and published slip rate data (Fig. 6a). The slip rate on the Provo fault is used as the reference to which the other rates are normalised. The Provo rate was chosen because it is well-constrained (Machette et al., 1992). Overall, a good match between observed and predicted rates was found. The exception is the centrally located Salt Lake City (SLC) fault segment. The predicted rate (2.8 mm/year) is comparable with that found for the last 5 ky (1.1–2.5 mm/year) (DePolo, 1998), but is significantly greater than the average rate estimated for the entire Holocene (0.8 mm/year since 15–20 ky) (Fig. 6a). Our method provides insight into this discrepancy. The high rate predicted by our model arises from the large ratio of overall fault zone length (350 km) to the SLC fault length (39 km; lengths measured as straight line distances). The adjacent faults are nearly twice as long. The discrepancy cannot be attributed to the way in which the fault segment lengths have been defined because in the SLC area, segment lengths defined using independent criteria compare well (Anders and Schlische, 1994). Our model suggests that the higher rate measured for the last 5 ky is more representative of the long-term slip rate. One possible explanation for the low

whole-Holocene rate is that other faults in the immediate hanging wall to the main trace of the Wasatch were also active during the early Holocene. This idea could be tested by further field studies.

4.1.3. Gulf of Corinth, Greece

Another example studied here is the Gulf of Corinth, Greece, which is bounded on the south side by three extensional faults from west to east: Egion, Xylokastron and South Alkyonides (Figs. 6b and 7b). The data we discuss are published so our account is brief. The systematic variation in maximum throw and hanging wall bathymetry along the entire array appears to indicate that these faults are behaving as a single larger structure of ~110 km length (Fig. 7b). The individual faults are comparable in length (35–40 km). Thus, according to our model, the predicted slip rate on the two distal faults should be ~1/3 that of the central fault, which has been slipping at 7–11 mm/year in the Quaternary (Armijo et al., 1996). The hanging wall bathymetry is well explained by these relative slip rates: the deepest part of the gulf associated with the central fault, with a water depth about 3× greater than that adjacent to the centres of the distal faults. When measured slip rates are normalised to that of the Xylokastron fault, we find a good agreement for the other faults with a variety of values measured from geological and seismological studies (Fig. 6b; Armijo et al., 1996; Clarke et al., 1997; Collier et al., 1998). Furthermore, recent geodetic results published by Kahle et al. (2000) show a concentric pattern of dilational strain centred on the Xylokastron fault, diminishing to the east and west along-strike, again consistent with our prediction. However, other geodetic studies show a westward increasing pattern of relative geodetic site velocities (e.g. Clarke et al., 1997; Briole et al., 2000). Thus, whether the highest seismic hazard from normal faulting earthquakes exists at the centre or western end of the gulf is unclear. Our model favours the former. To determine the correct answer we feel that more work is needed, but our model has highlighted a discrepancy between existing seismic hazard assessments.

5. Variations across strike

As we have already shown, the process of growth by fault linkage imposes a constraint on the observed spacing of extensional structures showing contemporaneous activity. This is because as linkage and profile re-adjustment proceed they change the way total fault strain is partitioned across an extending region. In other words, for the regional strain rate to remain constant, the increase in rates of slip that occurs as a fault grows by linkage must be accompanied by cessation of activity in the foot wall and hanging wall areas (Gupta et al., 1998; McLeod et al., 2000). In many actively extending regions, as we have reviewed above, there is ample geomorphological and seismological evidence that not all optimally oriented normal faults are active (Jackson, 1999; McLeod et al., 2000; Sharp et al., 2000).

We therefore extend the modeling of along-strike slip rate variations (Section 4) to consider the spacing between *simultaneously active* faults along-strike. The strain represented by a fault of length, L, and down-dip width, W, depends on the geometric moment, $M_g = dA$ where fault plane area $A = LW$, and W depends on the thickness of the faulted layer (Kostrov, 1974). According to the displacement–length scaling relationship $d_1 = \gamma L_1$, faults of length L_1 represent a strain $M_g = \gamma L_1^2 W$, whereas the linked structure with a fully re-adjusted (self-similar) profile represents a strain $M_g = \gamma L_2^2 W$ (using $d_2 = \gamma L_2$; Fig. 2). Note that in Fig. 2 $L_2 = NL_1$. It follows that the strain accommodated by the fully developed linked fault system (with $d_2 = \gamma L_2$) is N times larger than for the unlinked faults, assuming W remains constant. In order for the regional strain rate to remain constant the spacing between those faults that remain active must change. For the model shown in Fig. 2, active fault spacing measured across strike near the centre of the linking array will gradually increase through time from x_1 to x_2 as the displacement profile of the fault re-adjusts from d_1 to d_2. The distance x_1 is the average fault spacing between the initial faults of length L_1. The distance $x_2 = x_1(L_2/L_1)$ is the maximum active fault spacing achieved, whereas near the tips of the linking array little change to the original spacing x_1 will occur. This calculation is shown for the simplified geometry illustrated in Fig. 2 but can be generalised to any fault array dimensions. It can also be modified to allow for changes in down-dip width, W, which may also occur during linkage. For example, if W increases as profile re-adjustment occurs, the maximum spacing x_2 will be underestimated by our approach.

5.1. Application

The above may provide a plausible explanation for the differences in active fault spacing between the Lazio–Abruzzo region of central Italy compared with central Greece (Fig. 7). In Lazio–Abruzzo, the ratio of total throw to length for individual L_1 faults is 0.03–0.07; see Fig. 4). The ratio of throw-to-length for the interacting, but as yet unlinked, fault array (of length $L_2 = 130$ km) is lower (0.016; see Fig. 4). The average spacing between faults in this area, which all show Holocene activity, is 10–15 km (i.e. $x_2 = x_1$). In contrast, throw-length ratios for the three faults bordering the Gulf of Corinth are in the range 0.08–0.14, significantly higher than the ratio for the entire array (5 km/110 km = 0.045). In contrast to the Lazio–Abruzzo area, recent fault activity in central Greece is largely confined to the Gulf of Corinth and the Gulf of Evia, which are 60–70 km apart. The regions between the two Gulfs, and that south of the Corinth Gulf contain faults, spaced c. 15 km apart, which show little or no Quaternary activity (Jackson, 1999).

Our preferred interpretation of these patterns is that

profile readjustment is at an incipient stage in central Italy, whereas in the Corinth area it is virtually complete. In order to test this idea we calculated the expected spacing between active faults for the Corinth area using the following parameters: $x_1 = 15$ km, $L_2 = 110$ km and $L_1 = 35$ km. We ignore variation in W as the L_1 segments are already much longer than the thickness of the brittle crust. Using these parameters, our calculations suggest that no active faults should exist for a distance of approximately 47 km either side of the Xylokastron fault, using $x_2 = x_1(L_2/L_1)$. With a presumed additional effect from the faults around the Gulf of Evia, this may explain the lack of active faults within an across-strike distance of 60–70 km from the centre of the Gulf of Corinth. Further evidence in support of our interpretation is shown by the cross-sections of the Corinth area (Fig. 7b). By comparing the two cross-sections, it is clear that active fault spacing is not constant along strike, but increases from the eastern end of the Gulf towards the centre, consistent with the above.

6. Discussion

Our approach differs significantly from the statistical analysis of Wesnousky (1999) in which a scaling relationship between slip rate and length is proposed. Moreover, Wesnousky's (1999) data came from high-strain-rate strike-slip plate boundaries, in particular California, New Zealand and Japan. Consequently, a direct quantitative comparison with our approach is not possible. The physical mechanism proposed by Cowie (1998b), does predict that some faults will grow rapidly and experience higher slip rates, whereas other neighbouring faults may grow much more slowly and may even become inactive. It is important to emphasise that rapid growth may manifest itself as *either* accumulation of displacement *or* tip propagation, not necessarily both. Thus, according to the model of Cowie (1998a,b), longer faults are likely to exhibit higher slip rates but the converse is not necessarily true. In the examples shown here the central segments of linking extensional arrays exhibit significantly higher rates than the distal segments even though there may be no variation in segment length. Fault interaction and its control on slip rates, as discussed by Cowie (1998b), is implicit to our modelling approach, whereas the scaling relationship derived by Wesnousky's (1999) is entirely empirical.

A possible weakness in our model is the assumption that the L_1 faults develop at the same time and thus that interaction begins simultaneously along the length of the entire array. McLeod et al. (2000) describe a more complex sequence of subtle interaction effects prior to linkage that controls small local changes in the rates of growth of adjacent segments and the time sequence of linkage. Contreras et al. (2000) also found a complex pattern of shifting fault activity along-strike during the earliest stages of fault development (see their Fig. 5). There is no explanation for this given by Contreras et al. (2000) but it is possible that interactions were occurring during this period with other faults outside their study area. Our model focuses on the interactions between nearby faults forming an incipient array and neglects potential interactions with other, more distant, faults or fault arrays. Although these long-range effects are of low amplitude they may well be important in fault pattern development (Cowie et al., 1993).

Finally, we avoid making statements in this paper concerning the earthquake magnitudes or recurrence intervals that might be expected as a consequence of the predicted slip rates. Increased rates of slip can be achieved either by a decrease in recurrence interval or by an increase in magnitude or some combination of both. The example shown in Fig. 1 indicates that subsequent to hard linkage the segment boundaries do not act as persistent barriers to rupture (McLeod et al., 2000). Thus larger magnitude earthquakes (or compound earthquakes) are more likely post-linkage simply because the potential rupture area is increased. The negative correlation between earthquake stress drop and slip rate identified by Anderson et al. (1996) may also be relevant in this context because of the temporal increase in slip rate that accompanies linkage.

7. Conclusions

We have shown that simple fault scaling arguments may be used to model the spatial systematics of long-term slip rate within extensional fault arrays. In particular, variations in the displacement–length ratio associated with growth by linkage imply variations in slip rate along strike and through time. These slip rate variations must be accommodated by a change in the across-strike spacing between active structures in order to maintain a constant regional extension rate. Specific conclusions of our work include the following:

1. The variation in slip rate along-strike of a linking fault array depends on the original lengths and displacements of segments comprising the array, as well as their relative positions.
2. The magnitude of variation can be estimated if the original segment lengths can be established (i.e. L_1 in Fig. 2), using the positions of intra-basin highs, and/or deflected striations, and/or local displacement minima. Variations in the down-dip dimension of the fault plane associated with growth by linkage may be incorporated into our modelling approach but is of secondary importance in the examples we have studied.
3. A linear approximation for calculating *relative slip rate* as a function of distance from the ends of an array adequately describes observed patterns. It results in a simple expression for the slip rate enhancement factor $E = 2R_i/L_i$ for each segment comprising the array, where L_i is the length of the ith segment and R_i is the distance of the segment mid-point from the nearest tip of

the overall array. Thus, for the most distal segments $E = 1$ and for all other segments $E > 1$ because $R_i > L_i/2$ for an array consisting of more than one segment. It is straightforward to modify our approach to allow for a non-linear variation along-strike. For the central segments of arrays there is little difference between using a linear rather than an elliptical profile shape.

4. Relative slip rates along-strike can be converted into absolute values if a measured rate at one point along the array is available.
5. Our calculations have been compared with measured rate variations for well-studied extensional fault systems. Overall, our calculations compare well with measurements. However, our calculations suggest that the Holocene slip rate along the Salt Lake City segment of the Wasatch fault, Utah, appears to be anomalously low. We predict a rate of approximately 2.8 mm/year, which is comparable with that estimated to have occurred over just the last 5 ky. Also, our calculations imply that the central rather than the western part of the Gulf of Corinth, Greece has the highest seismic hazard potential.
6. We have also shown how the magnitude of slip rate variation along-strike can be quantitatively related to the cross-strike distance between *contemporaneously active faults*. We find that, while fault spacing in general may be controlled by the thickness of the brittle crust as previous authors have suggested, the distance between *active* structures may be greater than this. This pattern becomes more prominent as the displacement profile for interacting fault arrays re-adjusts to achieve a displacement–length ratio self-similar with pre-linkage segments. This is a testable prediction of our model that we have explored via a preliminary comparison of fault arrays in central Greece and the Lazio–Abruzzo area of Italy. Our results suggest that displacement profile re-adjustment is further developed in central Greece compared with Lazio–Abruzzo. A further testable prediction of the model is that *active fault spacing* should vary along strike, being greatest if measured at the centre of interacting fault arrays and decreasing towards the array tips.
7. The variations in slip rate and active fault spacing that we describe are consistent with the underlying physics of elastic interaction that is, in turn, controlled by structural segmentation inherited from the growth-by-linkage process. Thus, we believe that our approach may lead to an improvement of existing techniques for long-range earthquake hazard assessment because it implicitly includes the role of fault interactions, in addition to regional tectonic loading, in controlling fault slip rates.

Acknowledgements

This work was funded by a Royal Society of London University Research Fellowship to P. Cowie, and NERC GR9/02995 and Birkbeck College grants to G.P. Roberts. The Benfield Greig Hazard Research Centre at UCL is thanked for support. This work benefited from discussions with Alessandro Michetti, Nigel Morewood, Oona Scotti and Nancye Dawers. Reviews by Mark Anders and Juliet Crider, Jim McCalpin, Joe Cartwright and two anonymous reviewers improved the paper.

References

Anders, M.H., Schlische, R.W., 1994. Overlapping faults, intrabasin highs, and the growth of normal faults. Journal of Geology 102, 165–180.

Anders, M.H., Geissman, J.W., Piety, L.A., Sullivan, J.T., 1989. Parabolic distribution of circumeastern Snake River Plain seismicity and latest Quaternary faulting: migratory pattern and association with the Yellowstone hotspot. Journal Geophysical Research 94, 1589–1621.

Anderson, J.G., Wesnousky, S.G., Stirling, M.W., 1996. Earthquake size as a function of fault slip rate. Bulletin of the Seismological Society of America 86, 683–690.

Armijo, R., Meyer, B., King, G.C.P., Rigo Papanastassiou, A., 1996. Quaternary evolution of the Corinth rift and its implications for the Late Cenozoic evolution of the Aegean. Geophysical Journal International 126, 11–53.

Briole, P., Rogi, A., Lyon-Caen, H., Ruegg, J.C., Papazissi, K., Mtsakaki, C., Balodimou, A., Veis, G., Hatzfield, D., Deschamps, A., 2000. Active deformation of the Corinth rift, Greece: results from repested Global Positioning System surveys between 1990 and 1995. Journal of Geophysical Research 105, 25605–25626.

Burgmann, R., Pollard, D.D., Martel, S.J., 1994. Slip distributions on faults: effects of stress gradients, inelastic deformation, heterogeneous host rock stiffness, and fault interaction. Journal of Structural Geology 16, 1675–1690.

Byrd, J.O.D., Smith, R.B., Geissman, J.W., 1994. The Teton fault, Wyoming: topographic signature, neotectonics and mechanisms of deformation. Journal of Geophysical Research 99, 20095–20122.

Caskey, S.J., Wesnousky, S.G., 1997. Static stress changes and earthquake triggering during the 1954 Fairview Peak and Dixie Valley earthquakes, Central Nevada. Bulletin of the Seismological Society of America 87, 521–527.

Cartwright, J.A., Trudgill, B.D., Mansfield, C.S., 1995. Fault growth by segment linkage: an explanation for scatter in maximum displacement and trace length data from the Canyonlands Grabens of SE Utah. Journal of Structural Geology 17, 1319–1326.

Cavinato, G.P., De Celles, P.G., 1999. Extensional basins in the tectonically bimodal central Apennines fold-thrust belt, Italy: response to corner flow above a subducting slab in retrograde motion. Geology 27, 955–958.

Clarke, P., Davies, R., England, P., Parsons, B., Billiris, H., Paradissis, D., Veis, G., Denys, P., Cross, P., Ashkenazi, V., Bingley, R., 1997. Geodetic estimate of seismic hazard in the Gulf of Korinthos. Geophysical Research Letters 24, 1303–1306.

Collier, R., Pantosti, D., D'Addezio, G., De Martini, P.M., Masana, E., Sakellariou, D., 1998. Paleoseismicity of the 1981 Corinth earthquake fault: Seismic contribution to extensional strain in central Greece and implications for seismic hazard. Journal Geophysical Research 103, 30001–30020.

Contreras, J., Anders, M.H., Scholz, C.H., 2000. Growth of a normal fault system: observations from the Lake Malawi basin of the east African rift. Journal of Structural Geology 22, 159–168.

Cowie, P.A., 1998a. Normal fault growth in three-dimensions in continental and oceanic crust. In: Buck, R., Delaney, P., Karson, J., Lagabrielle, Y. (Eds.). Faulting and Magmatism at Mid-Ocean Ridges. , pp. 325–348 AGU Monograph 106.

Cowie, P.A., 1998b. A healing–reloading feedback control on the growth rate of seismogenic faults. Journal of Structural Geology 20, 1075–1087.

Cowie, P.A., Scholz, C.H., 1992. Physical explanation for the displacement–length scaling relationship for faults using a post-yield fracture mechanics model. Journal of Structural Geology 14, 1133–1148.

Cowie, P.A., Shipton, Z.K., 1998. Fault tip displacement gradients and process zone dimensions. Journal of Structural Geology 20, 983–997.

Cowie, P.A., Vanneste, C., Sornette, D., 1993. Statistical physics model for the spatio-temporal evolution of faults. Journal Geophysical Research 98, 21809–21821.

Dawers, N.H., Anders, M.H., 1995. Displacement–length scaling and fault linkage. Journal of Structural Geology 17, 607–614.

Dawers, N.H., Underhill, J.R., 2000. The role of fault interaction and linkage in controlling syn-rift stratigraphic sequences: Stafjord East area, northern North Sea. Bulletin of American Association of Petroleum Geologists 84, 45–64.

Dawers, N.H., Anders, M.H., Scholz, C.H., 1993. Growth of normal faults: displacement–length scaling. Geology 21, 1107–1110.

Davies, R., England, P., Parsons, B., Billiris, H., Paradissis, D., Veis, G., 1997. Geodetic strain of Greece in the interval 1892–1992. Journal of Geophysical Research 102, 24571–24588.

DePolo, C.M., 1998. A Reconnaissance Technique for Estimating Slip Rates of Normal-Slip Faults in the Great Basin, and Application to Faults in Nevada, USA. PhD Thesis, University of Nevada, Reno.

DePolo, C.M., Anderson, J.G., 2000. Estimating the slip rate of normal faults in the Great Basin USA. Basin Research 12, 227–240.

DePolo, C.M., Clark, D.G., Slemmons, D.B., Ramelli, A.R., 1991. Historical faulting in the Basin and Range province, western north America: implications for fault segmentation. Journal of Structural Geology 13, 123–136.

Dorsey, R.J., Umhoefer, P.J., Falk, P.D., 1997. Earthquake clustering inferred from Pliocene Gilbert-type fan deltas in the Loreto basin, Baja California Sur, Mexico. Geology 25, 679–682.

Doutsos, T., Poulimenos, G., 1992. The geometry and kinematics of active faults and their seismotectonic significance in the western Corinth–Patras Rift (Greece). Journal of Structural Geology 14, 689–700.

Ellis, M.A., Densmore, A.L., Anderson, R.S., 1999. Development of mountainous topography in the Basin Ranges USA. Basin Research 11, 21–42.

Galadini, F., 1999. Pleistocene changes in the central Apennine fault kinematics: a key to decipher active tectonics in central Italy. Tectonics 18, 877–894.

Galadini, F., Galli, P., Giraudi, C., 1997. Geological investigations of Italian earthquakes: new paleoseismological data from the Fucino Plain (Central Italy). Journal of Geodynamics 24, 87–103.

Giraudi, C., Frezzotti, M., 1997. Late Pleistocene Glacial Events in the central Apennines. Quaternary Research 48, 280–290.

Gudmundsson, A., 2000. Fracture dimensions, displacements and fluid transport. Journal of Structural Geology 22, 1221–1232.

Gupta, A., Scholz, C.H., 2000. A model of normal fault interaction based on observations and theory. Journal of Structural Geology 22, 865–880.

Gupta, S., Cowie, P.A., Dawers, N.H., Underhill, J.R.U., 1998. A mechanism to explain rift-basin subsidence and stratigraphic patterns through fault array evolution. Geology 26, 595–598.

Hayward, N.J., Ebinger, C.J., 1996. Variations in along-axis segmentation of the Afar rift system. Tectonics 15, 244–257.

Hodgkinson, K.M., Stein, R.S., King, G.C.P., 1996. The 1954 Rainbow Mountain–Fairview Peak–Dixie Valley earthquakes: a triggered normal faulting sequence. Journal of Geophysical Research 101, 25459–25471.

Jackson, J., 1999. Fault death: a perspective from actively deforming areas. Journal of Structural Geology 21, 1003–1010.

Jackson, J., White, N., 1989. Normal faulting in the upper continental crust: observations from regions of active extension. Journal of Structural Geology 11, 15–36.

Kahle, H.-G., Cocard, M., Peter, Y., Geiger, A., Reilinger, R., Barka, A., Veis, G., 2000. GPS-derived strain field within the boundary zones of the Eurasian, African, and Arabian Plates. Journal of Geophysical Research 105, 23,353–23,370.

King, G., Ellis, M., 1990. The origin of large local uplift in extensional regions. Nature 348, 689–693.

Kostrov, V., 1974. Seismic moment and energy of earthquakes, and seismic flow of rock. Izv. Acad. Sci. USSR Phys. Solid Earth 1, 23–44.

Machette, M.N., Personius, S.F., Nelson, A.R., Schwartz, D.P., Lund, W.R., 1991. The Wasatch fault zone, Utah — segmentation and history of Holocene earthquakes. Journal of Structural Geology 13, 137–149.

Machette, M.N., Personius, S.F., Nelson, A.R., 1992. Paleoseismology of the Wasatch fault zone: A summary of recent investigations, interpretations and conclusions. US Geological Survey Professional Paper 1500, A1–A71.

McCalpin, J.P., 1993. Neotectonics of the northeastern Basin and Range Margin, western USA. Zeitschrift fur Geomorphologie N. F. 94, 137–157.

McCloskey, J., Bean, C.J., 1994. Temporally unstable recurrence of earthquakes due to breaks in fractal scaling. Science 266, 410–412.

McLeod, A., Dawers, N.H., Underhill, J.R., 2000. The propagation and linkage of normal faults: insights from the Strathspey–Brent–Statfjord fault array, northern North Sea. Basin Research 12, 263–284.

Michetti, A.M., Brunamonte, F., Serva, L., Vittori, E., 1996. Trench investigations of the 1915 Fucino earthquake fault scarps (Abruzzo, Central Italy): Geological evidence of large historical events. Journal Geophysical Research 101, 5921–5936.

Morewood, N.C., Roberts, G.P., 1999. Lateral propagation of the surface trace of the South Alkyonides fault, central Greece: its impact on models of fault growth and displacement–length relationships. Journal of Structural Geology 21, 635–652.

Morewood, N.C., Roberts, G.P., 2000. The geometry, kinematics and rates of deformation within an en echelon normal fault segment boundary, central Italy. Journal of Structural Geology 22, 1027–1047.

Morley, C.K., 1999. Patterns of displacement along large normal faults: Implications for basin evolution and fault propagation, based on examples from east Africa. Bulletin of the American Association of Petroleum Geologists 83, 613–634.

Nicol, A., Walsh, J.J., Watterson, J., Underhill, J., 1997. Displacement rates of normal faults. Nature 390, 157–159.

Pantosti, D., D'Addezio, G., Cinti, F., 1996. Paleoseismicity of the Ovindoli–Pezza fault, central Apennines, Italy: a history including a large, previously unrecorded earthquake in the Middle Ages (860–1300 A.D.). Journal of Geophysical Research 101, 5937–5960.

Peacock, D.C.P., Sanderson, D.J., 1991. Displacements, segment linkage and relay ramps in normal fault zones. Journal of Structural Geology 13, 721–733.

Piccardi, L., Gaudemer, Y., Tapponier, P., Boccaletti, M., 1999. Active oblique extension in the central Apennines (Italy): evidence from the Fucino region. Geophysical Journal International 139, 499–530.

Poulimenos, G., 2000. Scaling properties of normal fault populations in the western Corinth Graben, Greece: implications for fault growth in large strain settings. Journal of Structural Geology 22, 307–322.

Roberts, G.P., 1996. Variations in fault-slip directions along active segmented normal fault systems. Journal of Structural Geology 18, 835–845.

Roberts, G.P., Ganas, A., 2000. Fault slip directions in central and southern Greece measured from striated and corrugated fault planes: comparison with focal mechanisms and geodetic data. Journal of Geophysical Research 105, 23443–23462.

Schlische, R.W., Young, S.S., Ackermann, R.V., Gupta, A., 1996. Geometry and scaling relations of a population of very small rift-related faults. Geology 24, 683–686.

Scholz, C.H., Contreras, J.C., 1998. Mechanics of continental rift architecture. Geology 26, 967–970.

Sharp, I.R., Gawthorpe, R.L., Armstrong, B., Underhill, J.R., 2000. Propagation history and passive rotation of mesoscale normal faults:

Implications for syn-rift stratigraphic development. Basin Research 12, 285–306.

Sieh, K., Stuiver, M., Brillinger, D., 1989. A more precise chronology of earthquakes produced by the San Andreas fault in southern California. Journal of Geophysical Research 94, 603–623.

Wallace, R.E., 1987. Grouping and migration of surface faulting and variations in slip rates on faults in the Great Basin Province. Bulletin of the Seismological Society of America 77, 868–876.

Wesnousky, S.G., 1999. Crustal deformation processes and the stability of the Gutenberg–Richter relationship. Bulletin of the Seismological Society of America 89, 1131–1137.

Willemse, E.J.M., 1997. Segmented normal faults: Correspondence between three-dimensional mechanical models and field data. Journal of Geophysical Research 102, 675–692.

Willemse, E.J.M., Pollard, D.D., Aydin, A., 1996. Three-dimensional analysis of slip distributions on normal fault arrays with consequences for fault scaling. Journal of Structural Geology 18, 295–309.